Ab-initio Calculations to Predict Stress Effects on Defects and Diffusion in Silicon

Milan Diebel
Department of Physics
University of Washington
Seattle, WA 98195, USA
Email: diebel@u.washington.edu

Scott T. Dunham
Department of Electrical Engineering
University of Washington
Seattle, WA 98195, USA
Email: dunham@ee.washington.edu

***Abstract*— Stress effects play an increasing role in processing and performance of current nanoscale ULSI devices. In this paper, we show how first principle calculations can be used to predict stress effects on equilibrium concentration and diffusion of defects in silicon. The method used is capable of treating arbitrary strain states, which is an extension beyond the hydrostatic case. For biaxial strain, we find strongly anisotropic diffusion of interstitials (I). We also extended our analysis to B and found similar behavior, leading to the prediction of enhanced lateral diffusion in strained Si on SiGe structures.**

I. Introduction

As ULSI devices enter the nanoscale, stress effects become more important as steep doping gradients and heterointerfaces induce stress gradients and reduced dimensions make any variation in diffusivity critical. On top of this, stress is induced purposefully to enhance carrier mobility [2]. Since experiments are difficult and in the case of boron diffusion lead to contradictory results [1], we utilize *ab-initio* calculations to predict stress effects on the formation and migration of point-defects and dopant/defect complexes which control dopant diffusion as well as dopant activation. In contrast to previous work, our analysis extends beyond simple hydrostatic activation volumes [3] in order to be able to predict anisotropies associated with more complex stress states (e.g. differences between in-plane and perpendicular diffusion due to biaxial strain). We determine both strain tensors as well as changes in elastic constants due to defects and migration saddle points.

II. Method

The elastic constants $C_{\alpha\beta}$ of a given material relate a stress/strain state to its energy:

$$E = \frac{1}{2}\sum_{\alpha}\epsilon_\alpha\sigma_\alpha = \frac{1}{2}\sum_{\alpha,\beta}\epsilon_\alpha C_{\alpha\beta}\epsilon_\beta. \quad (1)$$

Thus, once the elastic constants and induced strain for a given equilibrium structure or transition state are known, the change in formation E_f and migration energy E_m can be calculated, which leads directly to modified equilibrium concentrations and diffusivities. For our calculations we used the density functional theory (DFT) code VASP [9] with ultrasoft Vanderbilt type pseudopotentials [10]. All calculations were performed in general gradient approximation (GGA) with a 64 silicon atom supercell and a 2^3 Monkhorst-Pack **k**-point sampling. The energy cut-off was 200eV for pure Si structures with the exception of the I transition state, which was calculated with 150eV. The cut-off for structures including B was 340eV.

The elasticity tensor for the different structures (e.g. Si, I, and V) is determined by calculating the energy change for strain applied in different directions (hydrostatic, x-, y-, and z-direction). Different strains are applied by changing the lattice constant in a particular direction, while the lattice constant is kept fixed in all other directions. The systems are not under pure uniaxial stress, since relaxation due to the Poisson ratio ν is not allowed. By combining the results of straining the system in different directions, the elasticity constants $C_{\alpha\beta}$ and modified equilibrium lattice dimensions can be extracted.

III. Stress effect on defect formation energies

Figure 1 shows the energy versus hydrostatic strain for pure Si, a <110> split interstitial (I_{split}), and a vacancy (V). The data shown in Figs. 1 and 2 enable the calculation of the bulk modulus (K), the Young's modulus (E), and the Poisson's ratio (ν) of Si, all of which are in excellent agreement with experimental data (Table III). Table I and II list the data extracted from Figs. 1 and 2 respectively. The calculations show that the dominant effect of stress in the case of I and V is to modify the equilibrium lattice dimensions. In contrast, the difference in the curvatures and the resulting change in $C_{\alpha\beta}$ have a secondary effect.

System	a [eV/Å^2]	b_0 [Å]
Si	112.839	5.4578
I_{split}	100.361	5.4754
V	96.8374	5.4389

TABLE I
Assuming linear elastic behavior, the data shown in Fig. 1 can be fitted to $E(b) = E_0 + a(b - b_0)^2$.

Since the equilibrium lattice constant for Si depends on the point-defect concentration, it is convenient to use the following parameterization:

$$C_{\alpha\beta} \rightarrow C^{Si}_{\alpha\beta} + x_{I,V}\Delta C^{I,V}_{\alpha\beta}, \quad (2)$$

$$\epsilon_\alpha \rightarrow \epsilon_\alpha + x_{I,V}\epsilon^{I,V}_\alpha. \quad (3)$$

0-7803-7826-1/03/$17.00 © 2003 IEEE

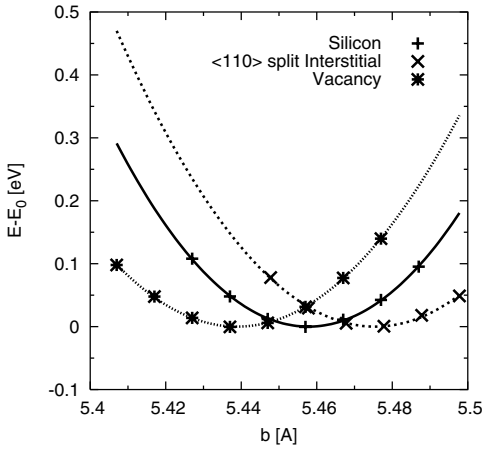

Fig. 1. Energy vs. unit cell lattice constant b for hydrostatic strain for system with $2 \times 2 \times 2 = 8$ cells (64 Si atoms in defect-free system). The reference energy E_0 is defined as the minimum energy as function of unit cell size. Vacancies (V) prefer the lattice constant to be reduced by 0.3% in comparison to Si, whereas interstitials (I) show the opposite behavior, with the lowest energy configuration a 0.3% increased lattice constant.

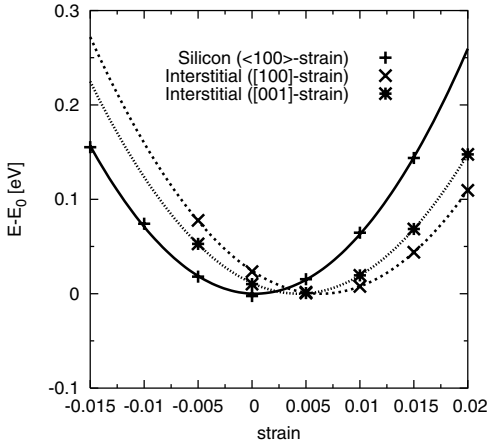

Fig. 2. Energy vs. uniaxial strain in different directions for Si and $\mathrm{I_{split}}$ oriented in the [110] direction. The reference energy E_0 is defined as the minimum energy for a given configuration.

where ϵ_α is the strain applied in reference to unstrained silicon and $x_{I,V} = C_{I,V}/C_S$ denotes the relative defect concentration. In this work, $x = 1/64$ since our supercell contains 64 Si lattice sites. Using Table I and II the elastic constants $C_{\alpha\beta}$ can be calculated for Si, V, and $\mathrm{I_{split}}$. The results are shown in Table III and IV. Our results indicate that in addition to inducing strain, vacancies and to a lesser extent interstitials soften the lattice (Table I and IV).

The knowledge of the elastic constants enables calculation of the formation energy of a defect for any strain state. Strain effects for vacancies are isotropic. However, since <110> split interstitials induce the largest strain in the x- and y-directions (Fig. 2), uniaxial or biaxial strain can lead to larger changes in the equilibrium point-defect concentration than would be predicted based on the hydrostatic activation volume. Figure 3 shows the stress dependence of the equilibrium interstitial

System under strain (uniaxial or shear)	a [eV]	$\epsilon_0[10^{-3}]$
Si (<100>-strain)	668.903	0.301
Si (shear strain)	360.374	5.35×10^{-4}
V (<100> strain)	517.685	-6.203
V (shear strain)	298.446	-2.2×10^{-3}
$\mathrm{I_{split}}$ ([100]-strain)	593.507	6.405
$\mathrm{I_{split}}$ ([001]-strain)	601.717	4.330

TABLE II

ASSUMING LINEAR ELASTIC BEHAVIOR, THE DATA SHOWN IN FIG. 2 CAN BE FITTED TO $E(\epsilon) = E_0 + a(\epsilon - \epsilon_0)^2$.

Silicon Property	DFT	Literature	
C_{11} [GPa]	164.8	166	Ref. [5], [6]
C_{12} [GPa]	55.6	64	Ref. [5], [6]
$E_{<100>}$ [GPa]	136.8	130	Ref. [5], [6]
$\nu_{<100>}$	0.252	0.278	Ref. [5], [6]
K [GPa]	92	97	Ref. [7], [8]

TABLE III

COMPARISON OF DFT RESULTS FOR C_{ij}, YOUNG'S MODULUS (E), POISSON'S RATIO (ν), AND BULK MODULUS (K) FOR SI WITH EXPERIMENTAL DATA. E AND ν ARE NOT INDEPENDENT PROPERTIES, SINCE THEY ARE DIRECTLY RELATED TO C_{11} AND C_{12}. THEY ARE JUST LISTED FOR THE CONVENIENCE OF THE READER.

concentration (C_I^*) under biaxial strain. Only the dominant effect due to the induced strain (difference in lattice dimension due to I incorporation) is included. In the dilute approximation, the formation energy for I can be written as:

$$E_I^f(\vec{\epsilon}) = E_I^f(0) + \Delta E_I^f(\vec{\epsilon}) = E_I^f(0) + \Omega\, \vec{\epsilon}_I \cdot (C_{Si} \cdot \vec{\epsilon}), \quad (4)$$

where $\vec{\epsilon}_I$ is the induced strain vector, $\vec{\epsilon}$ is the applied strain vector, C_{Si} is the elasticity tensor for Si, and Ω is the Si atomic volume.

In the case of biaxial strain:

$$\frac{C_I^*(\epsilon)}{C_I^*(0)} = \frac{1}{3}\exp\left(\frac{-\Delta E_{\mathrm{in}}^f(\epsilon)}{kT}\right) + \frac{2}{3}\exp\left(\frac{-\Delta E_{\mathrm{out}}^f(\epsilon)}{kT}\right), \quad (5)$$

where E_{in}^f is the change in energy for in-plane interstitials (e.g. [110] or [−110] orientation for strain in x-y plane), whereas E_{out}^f is the change for split interstitials with out of plane components (e.g., [011] orientation). Figure 3 shows a strong strain dependence of C_I^*, particularly for in-plane [110] interstitials. Interstitials prefer to be oriented in-plane under tensile strain and out of plane under compressive strain.

IV. STRESS EFFECTS ON DEFECT AND B DIFFUSION

Stress effects are even larger and more anisotropic for the I transition state. Figure 4 shows the transition barriers for interstitial migration in unstrained silicon calculated using the nudged elastic band method (NEB). Interstitial migration occurs via a two step process [4] (see Fig. 4). First, an interstitial moves from a split site to a hexagonal site ($\mathrm{I_{split}} \rightarrow \mathrm{T_1} \rightarrow \mathrm{I_{hex}}$), while passing through the transition

0-7803-7826-1/03/$17.00 © 2003 IEEE

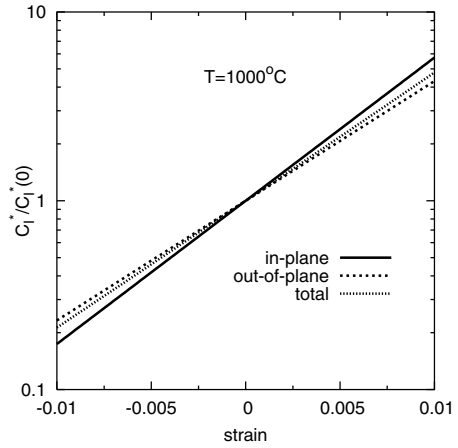

Fig. 3. Strain dependence of $C_I^*(\epsilon)/C_I^*(0)$ in biaxially strained Si at $T = 1000°C$. For strain applied in the x-y plane, 1/3 of all <110> interstitials are purely in-plane, while 2/3 have out of plane components. The plot shows the contributions from the different alignments and the resulting total.

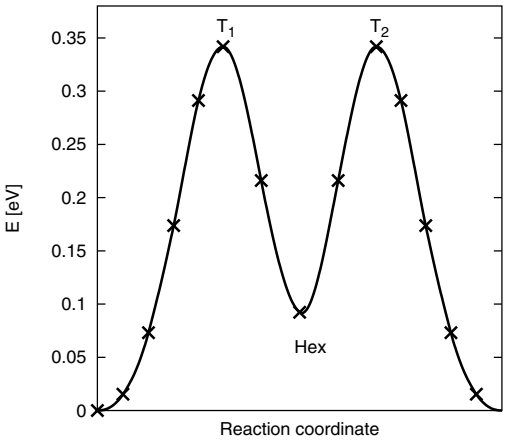

Fig. 4. Migration path for $\mathrm{I_{split}} < 110 > \rightarrow \mathrm{I_{hex}} \rightarrow \mathrm{I_{split}} < 110 >$ transition in unstrained Si. Due to the symmetry of the transition, $\mathrm{T_1}$ and $\mathrm{T_2}$ are equivalent configurations.

Elastic Constant	$\Delta C_{\alpha\beta}$ [GPa]
$\Delta C_{11}^V = \Delta C_{22}^V = \Delta C_{33}^V$	-2387.2
$\Delta C_{12}^V = \Delta C_{13}^V = \Delta C_{23}^V$	-57.6
$\Delta C_{11}^I = \Delta C_{22}^I$	-1190.4
ΔC_{33}^I	-1062.4

TABLE IV

CHANGE IN ELASTIC CONSTANT IN COMPARISON TO SI DUE TO INCORPORATION OF V AND $\mathrm{I_{split}}$.

System in uniaxial strain	a [eV]	$\epsilon_0[10^{-3}]$
$\mathrm{I_{trans}}$ ([100]-strain)	540.716	11.3549
$\mathrm{I_{trans}}$ ([010]-strain)	577.472	5.71637
$\mathrm{I_{trans}}$ ([001]-strain)	568.861	7.19477
$\mathrm{V_{trans}}$ ([100]-strain)	540.883	-10.3011

TABLE V

ASSUMING LINEAR ELASTIC BEHAVIOR, THE DATA SHOWN IN FIG. 5 CAN BE FITTED TO $E(\epsilon) = E_0 + a(\epsilon - \epsilon_0)^2$.

state $\mathrm{T_1}$. The second step consists of moving from the hexagonal site back to a split site ($\mathrm{I_{hex}} \rightarrow \mathrm{T_2} \rightarrow \mathrm{I_{split}}$). Since the transition is symmetric, the transition states $\mathrm{T_1}$ and $\mathrm{T_2}$ are equivalent configurations. Similar to the calculations discussed above, we calculated the energy change of these transition states with respect to applied strain. The results as shown in Fig. 5 and Table V indicate a strong anisotropy in the strain interactions.

In order to account quantitatively for strain effects, the two step transition needs to be considered. The different spatial orientations of the transition states $\mathrm{T_1}$ and $\mathrm{T_2}$ with respect to the applied strain are responsible for the anisotropic diffusion behavior. Each I site is surrounded by 12 hexagonal sites. The orientation of the transition state, and therefore the hop direction, determine the transition rate to each hexagonal site:

$$\Gamma_i = \Gamma_0 \exp\left[\frac{-\Delta E_i^m(\vec{\epsilon})}{kT}\right], \tag{6}$$

where Γ_0 is the transition rate in unstrained Si and $\Delta E_i^m(\vec{\epsilon})$ is the energy change of the i's migration barrier due to the present strain. Each hexagonal site is surrounded by six I sites. The rates Γ_j from the hexagonal site to the final I location determine the probability p_j for each process. Knowing the displacement from the initial I site Δx_j^2 and neglecting correlation between subsequent two-step ($\mathrm{I_{split}} \rightarrow \mathrm{T_1} \rightarrow \mathrm{I_{hex}}$) hops, the diffusivity in the x-direction can be written as:

$$D_x = \frac{1}{2}\sum_{i=1}^{12}\Gamma_i\left(\sum_{j=1}^{6} p_j \Delta x_j^2\right). \tag{7}$$

The other directions follow equivalently. p_j is defined by:

$$p_j = \frac{\Gamma_j}{\sum_{i=1}^{6}\Gamma_i}. \tag{8}$$

$\Delta E_i^m(\vec{\epsilon})$ is assumed to have the form of Eq. 4. To simplify the analysis, the transition state was assumed to be independent of the initial orientation of the interstitial. This implies that for a hop in the <311> direction, the induced strain for $\mathrm{I_{trans}}$ in the y- and z-direction should be equal. Therefore the average value from Table V was used.

Summing up all contributions in Eq. 7 for the in-plane and out-of-plane directions leads to the anisotropy in the diffusivity as a function of biaxial strain as shown in Fig. 6. Biaxial tension (as in strained Si on SiGe) leads to significantly higher in-plane diffusion compared to the perpendicular direction, with lateral diffusivity predicted to be approximately 50% higher than vertical diffusion for 1% tensile strain.

Boron, which has a similar migration path is expected to behave similarly to I, with significant consequences for the ability to control channel length and lateral abruptness. Figure 7 and Table VI show preliminary results for the boron transition state. The anisotropy (difference in components of

0-7803-7826-1/03/$17.00 © 2003 IEEE

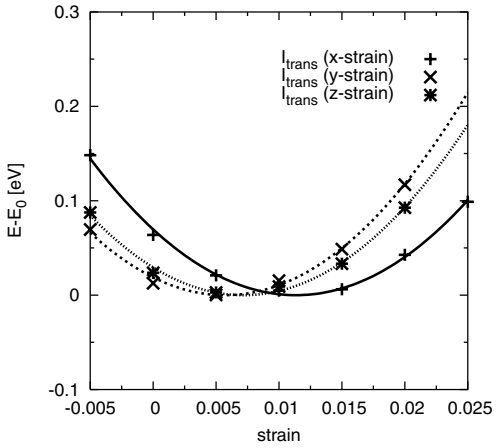

Fig. 5. Energy vs. uniaxial strain in different directions for the transition state of $\mathrm{I_{split}}[110] \rightarrow \mathrm{I_{hex}}$ with direction $(3/8, 1/8, 1/8)$. Note that the strain effect is largest in the dominant direction of motion.

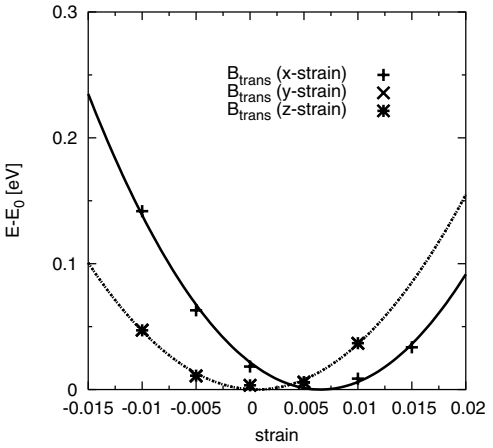

Fig. 7. Energy vs. uniaxial strain in different directions for the transition state of $\mathrm{B_s} + \mathrm{I_{tet}} \rightarrow \mathrm{B_{hex}}$ with hop vector $(3/8, 1/8, 1/8)b_0$. Note that the strain effect is largest in the primary direction of motion. The transition state behaves indentical under strain in the y- and z-direction.

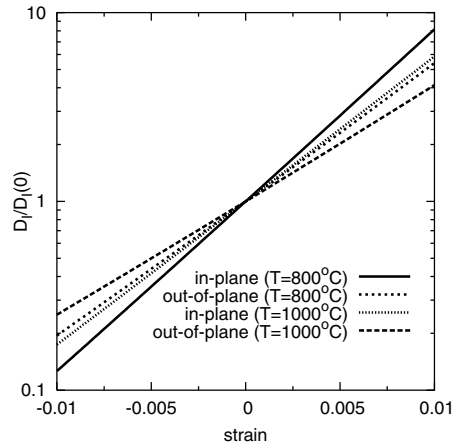

Fig. 6. Anisotropy of I diffusivity under biaxial strain. Shown are the in-plane and out-of-plane components at $T = 800°\mathrm{C}$ and $T = 1000°\mathrm{C}$ as a function of biaxial strain ϵ. $D_I(0)$ is the diffusivity in unstrained Si.

System in uniaxial strain	a [eV]	$\epsilon_0[10^{-3}]$
$\mathrm{B_{trans}}$ ([100]-strain)	505.919	6.546
$\mathrm{B_{trans}}$ ([010]-strain)	412.677	0.627
$\mathrm{B_{trans}}$ ([001]-strain)	411.923	0.629

TABLE VI

ASSUMING LINEAR ELASTIC BEHAVIOR, THE DATA SHOWN IN FIG. 7 CAN BE FITTED TO $E(\epsilon) = E_0 + a(\epsilon - \epsilon_0)^2$.

induced strain vector) is very similar to that calculated for I, and thus a similar strong anisotropy in B diffusion is anticipated.

V. CONCLUSION

We used *ab-initio* calculations to investigate the effect of stress on point-defect equilibrium concentrations and diffusivities. The calculations show a strong anisotropy in the case of I diffusion under biaxial strain. Similar effects are also seen in the case of B diffusion, with significant implications for controlling channel length and lateral abruptness.

ACKNOWLEDGMENT

This research was funded by the Semiconductor Research Corporation (SRC). The authors like to thank Intel Corporation for donation of a computing cluster used in this work.

REFERENCES

[1] M.S. Daw, W. Windl, N.N. Carlson, M. Laudon, and M.P. Masquelier, Phys. Rev. B **64**, 045205-1 (2001).

[2] K. Rim, J.L. Hoyt, and J.F. Gibbons, IEEE Transactions on Electron Devices, Vol. 47, No. 7, July 2000; J. Welser, J.L. Hoyt, J.F. Gibbons, IEEE Electron Device Letters, Vol. 15, No. 3, March 1994, p.100-102.

[3] M.J. Aziz, Appl. Phys. Lett. **70**, 2810 (1997).

[4] B. Uberuaga, Ph.D. thesis, University of Washington, Seattle, WA (2001).

[5] J.J. Wortman and R.A. Evans, J. Appl. Phys. **31**, 153 (1965).

[6] W.A. Brantley, J. Appl. Phys. **44**, 534 (1973).

[7] H. Elgamel, Sensors and Actuators A **50**, 17 (1995).

[8] Z. Djuric et al., Sensors and Actuators A **24**, 175 (1990).

[9] G. Kresse and J. Hafner, Phys. Rev. B **47**, RC558 (1993); G. Kresse and J. Furthmüller, **54**, 11169 (1996).

[10] D. Vanderbilt, Phys. Rev. B **41** 7892 (1990); G. Kresse and J. Hafner, J. Phys. Condens. Matter **6**, 8245 (1994).